SolarPACES 2023, 29th International Conference on Concentrating Solar Power, Thermal, and Chemical Energy Systems

Solar Fuels and Chemical Commodities

https://doi.org/10.52825/solarpaces.v2i.951

Published: 28 Aug. 2024

Supercritical Water Gasification of Biomass on CSP Plants: Comparison of On-Sun and Off-Sun Designs

Rafael Pérez-Álvarez[1,*], Alireza Rahbari[2], Armando Fontalvo[2], Shuang Wang[2], and John Pye[2]

[1] Department of Thermal and Fluids Engineering, University Carlos III of Madrid, Spain.

[2] School of Engineering, The Australian National University, Australia.

*Correspondence: rafperez@ing.uc3m.es

Abstract. A comparative study of On-Sun and Off-Sun designs for supercritical water gasification (SCWG) of biomass on concentrated solar power (CSP) plants was here presented. In the On-Sun design, the tubular reactor was placed on a cavity receiver of a solar power tower (SPT) plant and the heat employed to produce the gasification came directly from the sun (viz. the solar radiation was concentrated, thanks to the heliostat field, onto the tube's surface). In the Off-Sun designs, the gasification of the biomass was carried out inside a heat exchanger and it was produced thanks to the heat absorbed from the hottest fluid, which can be obtained from CSP plants or electrical heating. This work numerically investigated the thermomechanical performance of both designs. The results stood out the relation between temperature-gas yield-thermal stress. In On-Sun configurations the gas yield was 5 times higher than those obtained in the Off-Sun configuration. However, the highest values of both temperature and stress may produce the failure of the reactor. Fact that could be avoided in an Off-Sun reactor, since its uniform heating conditions mitigate the maximum temperature and stresses.

Keywords: SCWG of Biomass, Thermomechanical Modelling, Gasification on Solar Reactors.

1. Introduction

The world is facing an increasing demand for clean and renewable energy sources, and the use of biomass for energy production is one of the most promising options. Biomass gasification is a thermochemical process that converts biomass into a gaseous fuel. *Supercritical water gasification* (SCWG) uses water at high both pressure and temperature, above its critical point, as the gasification medium to convert biomass into syngas [1]. SCWG offers several advantages over conventional gasification methods, such as higher efficiency, faster reaction rates, and lower energy consumption [2]. It also has the potential to reduce the environmental impact of biomass conversion by producing a cleaner and more efficient fuel with lower greenhouse gas emissions. However, this technology still presents challenges, such as high reactor temperatures and pressures requiring advanced materials and design, or reactor blockages due to char/tar products.

Experimental measurements inside the SCWG reactor are challenging due to the extreme operating conditions, which limits the amount of information that can be obtained about the internal fluid flow, heat transfer, mass transfer, and reactions. Most authors in the literature only report the syngas composition and the temperature at the reactor's outlet. To complement the experimental analysis, *computational fluid dynamics* (CFD) simulation has emerged as a

powerful tool to provide valuable information about this process, that is difficult to obtain experimentally. By using CFD simulation, the flow patterns and temperature distribution inside the reactor, as well as the reaction kinetics and product formation rates can be analyzed. This information is essential for understanding the underlying mechanisms of the SCWG process and for optimizing the reactor design and operation.

Facing a sustainable production of liquid fuels, this work wants to analyze the combination of SCWG of biomass with renewable energy sources. *Concentrating solar power* (CSP) plants can supply heat for end-use applications or generate electricity through conventional power cycles. Thus, the heat required to produce biomass gasification could be proportioned by solar energy. Specifically, due to the temperatures required in this process, Solar Power Tower (SPT) technology has been chosen. Nevertheless, some key issues should be analyzed before asserting the feasibility of biomass gasification using CSP technologies, such as the overall cost of the process, materials compatibility, the combination with other devices of the plant, or the storage of energy to attenuate the variability of the solar resource. The investigation of cited topic could be structured into several tasks as detailed modeling of the solar reactor, design of the solar SCWG process, analysis of its annual performance, techno-economic feasibility of the plant, or lab-scale proof-of-concept reactor. The present work starts with the preliminary analysis of the solar reactor through detailed numerical simulations.

2. System description

A SCWG reactor typically consists of a high-pressure vessel, a heating system, and a gasification zone. The heating system provides the necessary thermal energy to heat the water to supercritical conditions. In the gasification zone, the biomass feedstock is introduced into the supercritical water where the gasification reaction is produced. The reaction generates a syngas stream mainly composed of hydrogen, carbon monoxide, methane, and carbon dioxide. The composition of this stream depends on the biomass employed. The syngas stream is then cooled and separated from the liquid products, such as organic acids and alcohols, by passing through a condenser and a series of separators. In this work, only the gasification zone is studied. For brevity, from this point, it is referred to as a reactor.

Two potential configurations appear here for solar reactors, as a function of whether the sun directly heats the reactor's tubes (On-Sun design) or an alternative heat transfer medium is employed instead (Off-Sun design).

- *On-Sun design*: the reactor is placed inside a cavity receiver, which is located at the top of the tower and surrounded by a heliostat field. The internal of the receiver/reactor consists of parallel tubes for transporting the HTF. Therefore, the heat employed to produce the gasification comes directly from the sun (viz. the solar radiation is concentrated onto the receiver tubes' surface thanks to the heliostat field). This configuration is similar to the current SPT plants but employs a different HTF. While the SPT plants devoted to producing electricity use molten salt or liquid sodium, the On-Sun reactor would employ a mixture of the supercritical water (s-H2O) and biomass solution.
- *Off-Sun designs*: This configuration accepts different ways to provide the energy required to perform the gasification, such as electrical heating or through a fluid heated with CSP technologies. Compared with On-Sun configurations, this design allows for mitigation of the fluctuations associated with the solar resources and heats more uniformly the reactors wall. In this work, the gasification of the biomass is produced inside a shell and tube heat exchanger. This configuration allows the inclusion of this kind of reactors on current SPT plants as a secondary system.

For the sake of brevity, the dimensions of the reactor’s tubes of both On-Sun and Off-Sun designs are the same (viz. DN15/SCH40 and length of 25 m) to compare its thermomechanical responses in each configuration. The main goal of the present work is to discuss the potential

benefits and disadvantages of the above-cited reactor configurations to produce syngas. Highlight that in future works, the design and optimization of solar reactors will be tackled.

3. Reactor modelling

3.1 Thermochemical characterization

CFD simulations were carried out to investigate numerically the glycerol gasification on SCWG. The model included reaction kinetics, transport phenomena, and both turbulence and radiation modeling. The mass, momentum, energy, and species conservation were solved using the Reynolds Average Navier-Stokes (RANS) equations, expressed in the steady-state, through the commercial software ANSYS Fluent. Different turbulent models were analyzed to obtain the closure of the momentum and energy RANS equations. In light of the discussion presented in Section 4.1, the $k-\varepsilon$ RNG turbulent model with Enhanced wall function was selected to perform the simulations. Discrete Ordinates was set as radiation model. All the before equations were discretized with a pressure-based finite volume method and were solved using the coupled algorithm. In addition, a Second-Order Upwind method was used to discretize all these equations. Solution iterations were stopped when the residuals of the equations reached a value below 10^{-6}. Moreover, both the gas yield composition and the HTF temperature at the reactor's outlet was monitored to confirm the stabilization of the solution.

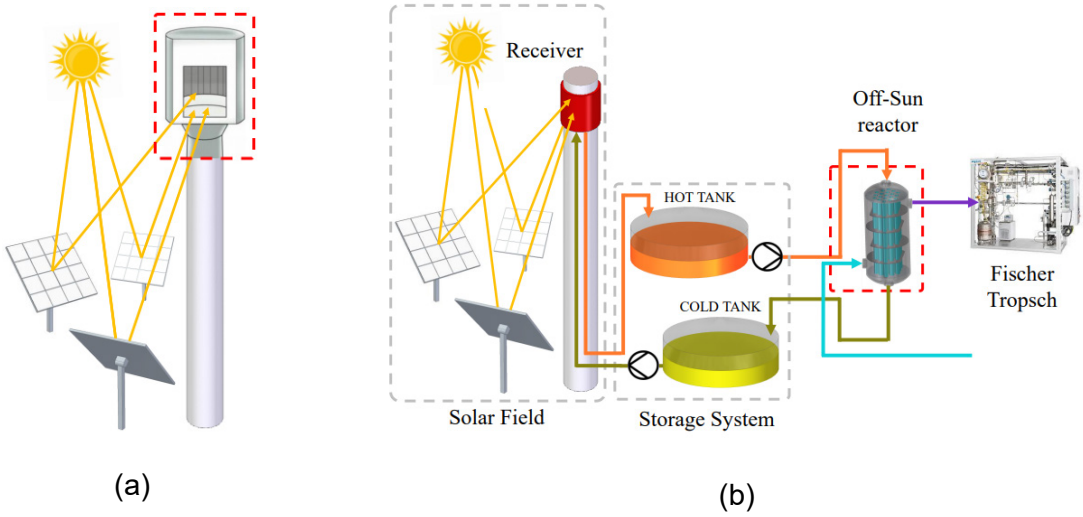

Figure 1. *Schematic representation of the studied solar reactors: (a) On-Sun design and (b) Off-Sun design.*

According to [1,3], due to the excess of water, the behavior of the gasification reaction can be represented through a pseudo-first-order kinetic. In [4,5], the authors experimentally observed that no char was produced during this reaction. Therefore, a homogeneus reacting flow was considered. Empirical reaction stoichiometry and kinetics of glycerol gasification, shown in Equations 1 and 2 respectively, were obtained from [6,7].

$$C_3H_8O_3 + 1.0781\ H_2O \rightarrow 4.441\ H_2 + 0.3186\ CH_4 + 1.2619\ CO + 1.4196\ CO_2 \quad (1)$$

$$k_r = 10^{5.9\pm1.3}(s^{-1}) \cdot e^{-\frac{104.5\pm20.3\ kJ/mol}{R\cdot T}} \quad (2)$$

Similar to [6], the reaction rate of glycerol gasification was assumed kinetically limited. Thus, Finite-Rate was used to characterize the turbulence-chemistry interaction. The physical properties of the pure water have been calculated by IAPWS-IF97 [8], while the properties of

the individual pure species have been obtained from Chung et al. [9] and from NASA thermodynamic database [10]. The mixture fluid properties were computed by mass-weigh average, except density which was estimated through Peng-Robinson EoS [11,12]. The change in composition of the supercritical phase with temperature and extent of reaction is accounted for at each point inside the reactor tube and the exit fluid is assumed to be a single phase supercritical mixture of syngas and H_2O. Supercritical conditions in the reactor inevitably impact the material constraints due to the confluence of high pressure and temperature, and corrosivity of the medium. Therefore, Haynes 230 was chosen for the material for reactor's tube since it combines excellent high-temperature strength, long-term thermal stability, and excellent low cycle fatigue properties at elevated temperature. Its properties were considered temperature dependence with the exception of its density, whose variation with temperature was comparatively much smaller than the rest of properties.

3.1.1 Boundary conditions of On-Sun design

The main boundary conditions of the On-Sun CFD model are described next. Mass flow rate, temperature, pressure and biomass concentration define the characteristics of the fluid mixture at the reactor's tube inlet. These are imposed through a mass flow-inlet condition with standard turbulence parameters. Similar to [13], temperature and pressure of $426ºC$ and $25\ MPa$ respectively were defined at tube's inlet. The concentrated solar radiation is used to increase the temperature of heat transfer fluid — $10\ wt.\%$ glycerol solution in this case — from $426°C$ to $625°C$ and also provide the endothermic heat for the gasification reactions. The mass flow-rate at reactor's inlet was modified to achieve the desired fluid temperature at outlet. At the tube exit, pressure-outlet conditions are selected for the fluid. The upper and lower cross-sections of the tube are regarded as adiabatic surfaces. A condition of non-slip is enforced for the velocity of the heat transfer fluid in contact with the wall surfaces. The heat flow on the surface of the tube in both the axial (z) and circumferential (θ) directions is not uniformly distributed due to the configuration and operation of SPT receivers. The heat absorbed on the front side of the tube is significantly greater than the insignificant amount absorbed on the back side (|θ|>90°). Thus, an adiabatic condition is applied at this zone. On the front side ($|\theta| \leq 90^o$), the heat flux absorbed, as described in Equation 3, is determined in the simulation code using a User-Defined Function (UDF) [14].

$$q''_{net} = \begin{cases} q''_{inc} - q''_{rad} - q''_{conv} & if\ |\theta| \leq 90^o \\ 0 & if\ |\theta| > 90^o \end{cases} \quad (3)$$

Where:

- Incident heat flux (q''_{inc}): it is calculated from Equation 4 using the concentrated heat flux obtained from optical simulations (q''_{con}).

$$q''_{inc} = q''_{con}(\theta, z) \cdot cos\theta \quad (3)$$

  As depicted Figure 2(a), a polar heliostat field, same as [15], was employed in this study. The heliostat field layout was established using SolarPILOT [16]. The system was ray-traced using SOLSTICE software for equinox noon conditions. The DNI was $1000\ W/m^2$. The specific aiming strategy used in this study was the MDBA method [17]. The aiming extend was chosen as 0.6 and the shape exponent was set as 1.5. Aiming points were dispersed vertically, while in horizontal direction, all heliostats aim on the centreline of the cavity. The resulting heat flux concentrated on tubes surfaces, q''_{con}, is depicted in Figure 2(b).
- Radiation losses (q''_{rad}): are calculated from Equation 5. The external radiation losses are estimated by calculating the emissivity (ε) locally as a function of tube temperature (T_w). An approximation was used based on experimental data available for Pyromark 2500 on cold-rolled steel [18]. This emissivity was further adjusted for cavity behaviour [19].

$$q''_{rad} = \varepsilon \cdot \sigma \cdot T_w^4 \quad (4)$$

- Convection losses (q''_{conv}): are calculated from Equation 6. The external convection losses from the cavity, as an approximation, can be assumed to be a function of the temperature difference between the tube wall (T_w) and the ambient air (T_{amb}) [20]. Correlation proposed by Leibfried and Ortjohann [21] was used here to estimate the total convective coefficient (h) for the heat loss from the cavity.

$$q''_{conv} = h \cdot (T_w - T_{amb}) \quad (5)$$

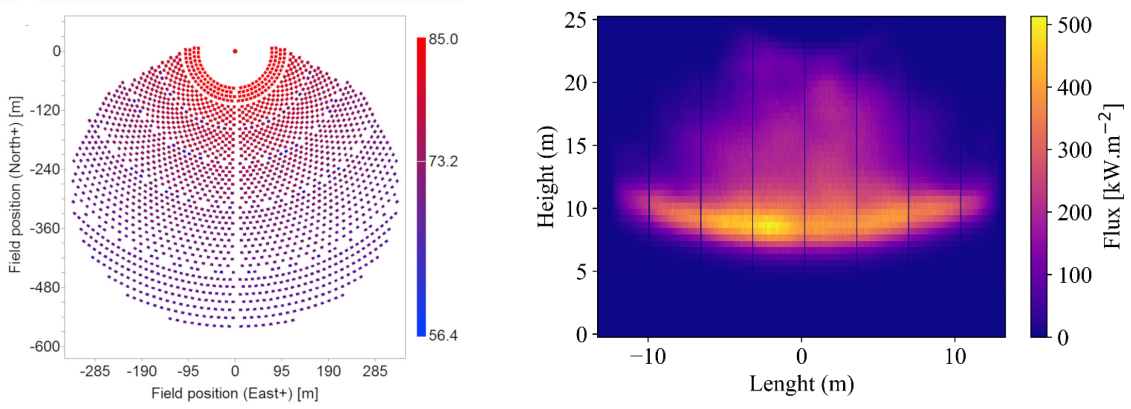

(a) (b)

Figure 2. *(a) Layout of the studied heliostat field [15], (b) Incident flux concentrated on the tubes' surface.*

3.1.2 Boundary conditions of Off-Sun design

Due to the complexity and the high computational cost of solving a whole heat exchanger, only a representative tube is investigated. Therefore, the modeling of both On-Sun and Off-Sun designs mainly differs from the heating conditions experienced by the outer tube surface, while the other boundary conditions are kept. In the Off-Sun design, the heat could be obtained from different sources. Here, the heat required for the gasification is provided by the hottest HTF (viz. high-temperature chloride salt). The heat absorbed by the Off-Sun reactor is described in Equation 7, and it is computed from the overall heat transfer coefficient (U) and temperature difference between the chloride salt and mixture, $\bar{T}_{salt}$ and $T_{mixture}$ respectively. The convection coefficient for the counter-flow heat exchanger was obtained from [21] and it is expressed as Reynolds number of hottest HTF.

$$q''_{net} = U \cdot (\bar{T}_{salt} - T_{mixture}) \quad (6)$$

3.2 Mechanical characterization

Reactor tubes are exposed to high pressures and nonuniform temperature distribution. Then, its stresses can be classified into mechanical and thermal stresses:

- Thermal stress: it is produced by the nonuniform temperature distribution on reactor walls. The characterization was done through the analytical methodology presented by [23]. This methodology calculated the elastic thermal stresses of tubes under a non-axisymmetrical temperature distribution and steady- or quasi-steady-state conditions. This methodology needed the temperature field obtained from the CFD model. In this

work, *generalized plane strain* (GPS) conditions were considered since they were an excellent approach to the receiver tube displacement when clips restrict it [23]. Through GPS conditions only the free axial expansion of the tubes was allowed. Although these conditions are representative of On-Sun design, may not be for the Off-Sun configuration. For the sake of brevity, GPS conditions have also been employed for Off-Sun design, resulting in a conservative mechanical study for this configuration. Future works will tackle the design and detailed mechanical characterization of Off-Sun reactors.

- Mechanical stress: it is generated by the pressure loads. Using the methodology proposed by [24], for and axially unconstrained tube the mechanical stresses depend only by pressure loads and reactors dimension. As mentioned, the operating pressure and the reactor dimensions are the same in both On-Sun and Off-Sun designs. Then, according to [24] mechanical stresses would be similar in both configurations, doing that the main differences between these designs, from mechanical point of view, reside in thermal stresses. Thus, only thermal stresses are reported in the results section.

4. Results

4.1 Model verification

Before discussing the thermomechanical performance of both On-Sun and Off-Sun configurations, the thermochemical model is verified through the comparison with the results presented in [13]. In addition, four turbulence models were compared to find which could accurately describe the SCWG process. The comparison of experimental gas yields with simulated gas yields is shown in Figure 3 for different reactor wall temperatures: 600ºC, 650ºC, and 700ºC. A good agreement is observed between the CFD model and the experimental. Additionally, the turbulence model $k-\varepsilon$ RNG was chosen since averagely fits better with experimental results. This fact fits with those observed in other works, which recommended this turbulent model to calculate the heat transfer of SCW in circular cross-section tubes.

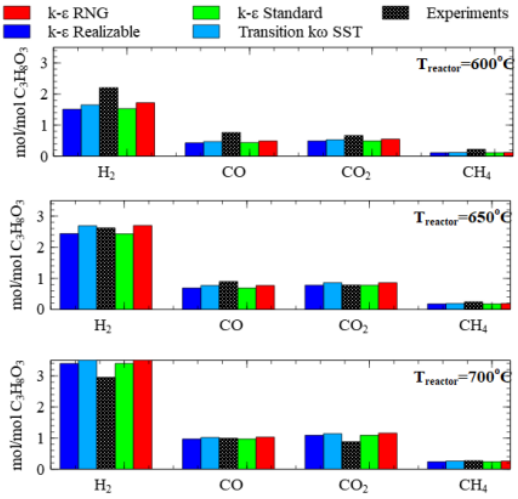

Figure 3. *Comparison of experimental gas yields with simulated gas yields.*

4.2 Comparison between On-Sun and Off-Sun configurations

Figure 4 and 5 show the main results obtained for both On-Sun and Off-Sun configurations. In light of the results, it can be asserted that the heating conditions rule the behavior of solar reactors. For the temperatures of the On-Sun configuration, the tubes' temperature peaked in the same place where the heat flux was maximum (see Figure 2(b)). Those tubes that received more heat flux, those located in front of the aperture (viz. panels 3-4-5-6), experienced higher temperatures and could generate more syngas but their thermal stresses were considerably

higher than panels with lower solar concentration. These enormous temperatures and stresses may produce bigger creep-fatigue damages, reducing considerably the solar reactor lifespan. The uniform heating experienced by the Off-Sun configuration drove a linear temperature change on their temperatures. The differences between tubes in this configuration are not so notorious as in the On-Sun reactor. This fact would allow easier control of the system. In addition, the uniform heating would permit the reduction of both temperature and thermal stress peaks. However, the syngas production in this configuration was 5 times lower than On-Sun design.

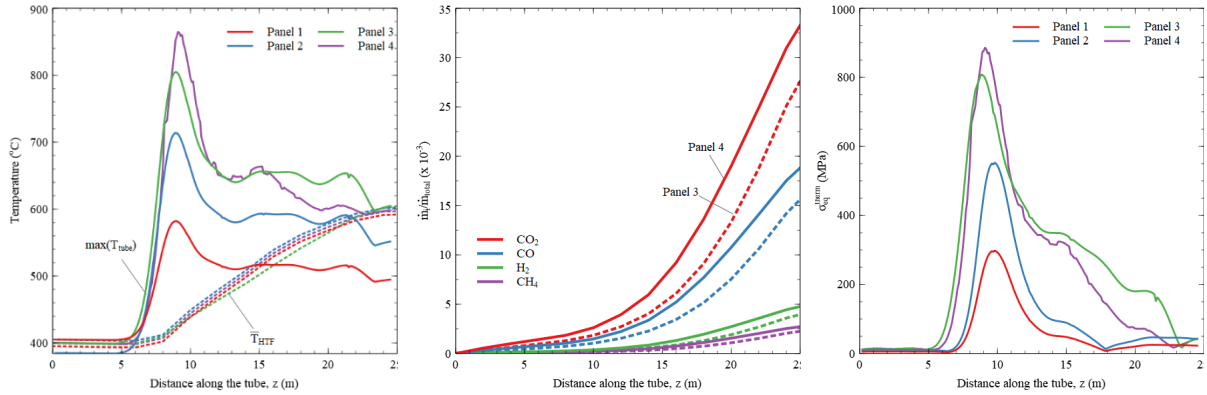

Figure 4. *For the On-Sun configuration. Axial distribution of: (a) temperature, (b) gas yield, and (c) thermal stresses.*

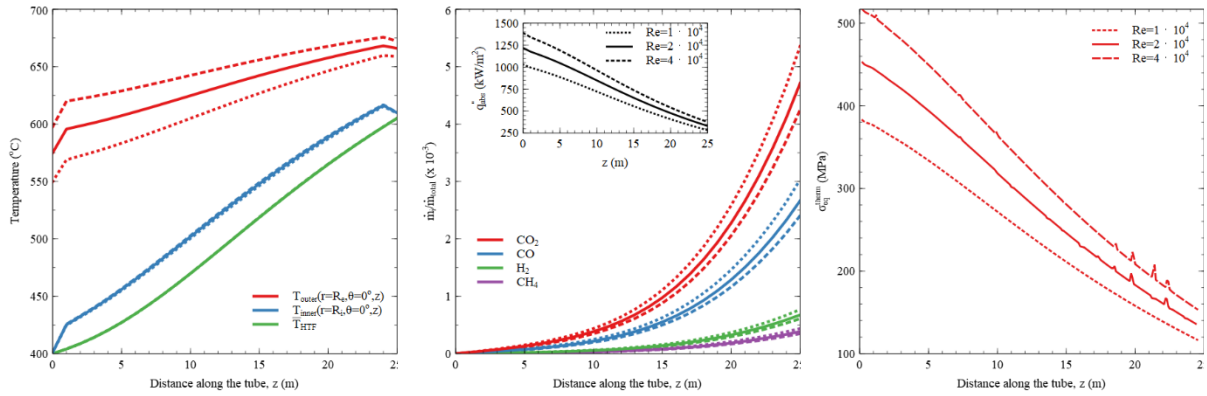

Figure 5. *For the Off-Sun configuration. Axial distribution of: (a) temperature, (b) gas yield, and (c) thermal stresses.*

5. Conclusions

A relation between temperature-gas yield-thermal stress was observed. Those designs that offer higher biomass conversion onto syngas (On-Sun) experienced excessive temperature and stresses. This fact could be solved through a uniformization of heating conditions, employing other designs of solar receivers, such as star receivers. For Off-Sun configurations, the gas yield conversion could be controlled through the feeding mass flow rate and the conditions of the hottest fluid employed to perform the heating although this fact implies an increase in the mechanical demand of the heat exchanger.

Author contributions

Rafael Pérez-Álvarez: Conceptualization, Methodology, Validation, Software, Writing – original draft, Writing – review & editing. Alireza Rahbari: Supervision, Conceptualization, Methodology, Writing – review & editing. Armando Fontalvo: Methodology, Writing – review & editing. Shuang Wang: Methodology, Validation, Software, Writing – review & editing. John Pye: Supervision, Conceptualization, Methodology, Writing – review & editing.

Competing interests

The authors declare that they have no known competing financial interests or personal relationships that could have appeared to influence the work reported in this paper.

Funding

Rafael Pérez-Álvarez acknowledges financial support from the European Union-NextGenerationEU and the Ministry of Universities and Recovery, Transformation and Resilience Plan of the Spanish Government through the "Margarita Salas grants for the training of young doctors" of the University Carlos III of Madrid and the financial support from the grant PID2021-122895OB-I00 funded by MCIN / AEI / 10.13039 / 501100011033 and by “ERDF A way of making Europe” and the grant TED2021-129326B-I00 funded by MCIN/AEI/ 10.13039/501100011033 and the European Union NextGenerationEU/PRTR.

References

1. Yakaboylu, O., Harinck, J., Smit, K. G., & De Jong, W. (2015). Energies, 8(2), 859-894. https://doi.org/10.3390/en8020859
2. Basu, P., and Vichuda M. International Journal of Chemical Reactor Engineering 7.1 (2009). https://doi.org/10.2202/1542-6580.1919
3. Lee, In-Gu, Mi-Sun Kim, and Son-Ki Ihm. Industrial & Engineering Chemistry Research 41.5 (2002): 1182-1188. https://doi.org/10.1021/ie010066i
4. Chakinala, Anand G., et al. Industrial & Engineering Chemistry Research 49.3 (2010): 1113-1122 https://doi.org/10.1021/ie9008293
5. Van Bennekom, J. G., et al. The Journal of Supercritical Fluids 58.1 (2011): 99-113. https://doi.org/10.1016/j.supflu.2011.05.005
6. Yukananto, R, Pozarlik, A.K and Brem, G. Journal of Supercritical Fluids 133 (2018): 330-342. https://doi.org/10.1016/j.supflu.2017.11.001
7. Guo, S., et al. International journal of hydrogen energy 37.7 (2012): 5559-5568 https://doi.org/10.1016/j.ijhydene.2011.12.135
8. Wolfgang, W. and Kretzschmar, H.. (2007). Springer Science & Business Media. ISBN: 3540742344.
9. Chung, Ting Horng, et al. Industrial & engineering chemistry research 27.4 (1988): 671-679. https://doi.org/10.1021/ie00076a024
10. Burcat, Alexander. Combustion chemistry (1984): 455-473.
11. Melhem, Georges A., Riju Saini, and Bernard M. Goodwin. Fluid Phase Equilibria 47.2-3 (1989): 189-237. https://doi.org/10.1016/0378-3812(89)80176-1
12. Stryjek, R., and J. H. Vera. The canadian journal of chemical engineering 64.2 (1986): 323-333. https://doi.org/10.1002/cjce.5450640224
13. Jin, Hui, et al. The Journal of Supercritical Fluids 107 (2016): 526-533. https://doi.org/10.1016/j.supflu.2015.06.028
14. Pérez-Álvarez, R., et al. (2023) Energy 283, 129170. https://doi.org/10.1016/j.energy.2023.129170
15. Venkataraman, Mahesh B., et al. AIP Conference Proceedings. Vol. 2126. No. 1. AIP Publishing, 2019. https://doi.org/10.1063/1.5117697

16. NREL, Solar PILOT, https://www.nrel.gov/csp/solarpilot.html, Accessed Aug, 2023,
17. Wang, Shuang, et al. Solar Energy 225 (2021): 694-707. https://doi.org/10.1016/j.solener.2021.07.059
18. Ho, Clifford K., et al. Journal of Solar Energy Engineering 136.1 (2014): 014502. https://doi.org/10.1115/1.4024031
19. Jilte, R.D., Kedare, S.B. and Nayak, J.K., 2013. Mechanical Engineering Research, 3(1), p.25. doi:10.5539/mer.v3n1p25
20. Siebers, Dennis L., and John S. Kraabel. United States (1984). https://doi.org/10.2172/6906848
21. Leibfried, U., and J. Ortjohann (1995): 75-84. https://doi.org/10.1115/1.2870873
22. Hausen, Helmuth. (1983). ISBN: 978-0070272156,
23. Laporte-Azcué, M., et al. Solar Energy 195 (2020): 355-368. https://doi.org/10.1016/j.solener.2019.11.066
24. S. Timoshenko, J. N. Goodier, Theory of Elasticity, by S. Timoshenko and J.N. Goodier, 2nd Edition, volume 49, McGraw-Hill Book Company, 1951